Two- and three-body photodissociation of gas phase I_3^-

Alexandra A. Hoops, Jason R. Gascooke,[a] Ann Elise Faulhaber, Kathryn E. Kautzman, and Daniel M. Neumark[b]
Department of Chemistry, University of California, Berkeley, California, 94720 and Chemical Sciences Division, Lawrence Berkeley National Laboratories, Berkeley, California 94720

(Received 2 September 2003; accepted 9 February 2004)

The photodissociation dynamics of I_3^- from 390 to 290 nm (3.18 to 4.28 eV) have been investigated using fast beam photofragment translational spectroscopy in which the products are detected and analyzed with coincidence imaging. At photon energies $\leqslant$3.87 eV, two-body dissociation that generates $I^- + I_2(A\,^3\Pi_{1u})$ and vibrationally excited $I_2^-(X\,^2\Sigma_u^+) + I(^2P_{3/2})$ is observed, while at energies $\geqslant$3.87 eV, $I^*(^2P_{1/2}) + I_2^-(X\,^2\Sigma_u^+)$ is the primary two-body dissociation channel. In addition, three-body dissociation yielding $I^- + 2I(^2P_{3/2})$ photofragments is seen throughout the energy range probed; this is the dominant channel at all but the lowest photon energy. Analysis of the three-body dissociation events indicates that this channel results primarily from a synchronous concerted decay mechanism. © *2004 American Institute of Physics.* [DOI: 10.1063/1.1691017]

I. INTRODUCTION

The tri-iodide anion, I_3^-, is a rare example of a molecule whose photodissociation dynamics have been studied in detail both in solution and in the gas phase, thereby presenting a unique opportunity for understanding how isolated, gas phase molecular photophysics can be modified by solvation effects. While much of the original work on I_3^- was performed in condensed phases, several recent gas phase experiments have provided significant insight into the energetics, spectroscopy, and photodissociation dynamics of this linear, closed-shell anion. However, experiments performed in different laboratories[1,2] suggest that significant questions remain regarding the primary photochemistry of the tri-iodide anion, particularly concerning the branching ratios among available product channels. In this paper, the photodissociation dynamics of I_3^- are investigated with an upgraded instrument in order to resolve this and other issues.

The spectroscopy and decay dynamics of I_3^- in solution have been examined extensively. Its absorption spectrum[3] comprises two broad bands centered at approximately 360 and 290 nm, henceforth referred to as the lower and upper bands, that have been assigned to transitions from the $^1\Sigma_g^+$ ground state to admixtures of $^3\Pi_{0+u}$ and $^1\Sigma_{0+u}$ excited states.[4–6] Raman spectra at laser frequencies resonant with either band show extended progressions in the I_3^- symmetric stretch,[7–10] indicating that initial nuclear motion in the upper states occurs along this coordinate. Ruhman and co-workers[11–14] and, more recently, Vohringer and co-workers[15–17] have used femtosecond laser techniques to probe the photodissociation of I_3^- in ethanol and other solvents via excitation of both electronic bands. Their findings revealed that the I_2^- photoproduct was generated within a few hundred fs in a coherent superposition of vibrational states with $\langle v\rangle \approx 12$. Additionally, evidence of I^- production via three-body dissociation was observed at 266 nm.[17] These experiments have stimulated several theoretical studies on the electronic states and photodissociation dynamics of I_3^-.[18–24]

In the gas phase, Do *et al.*[25] used collision-induced dissociation of I_3^- in a tandem mass spectrometer to determine a dissociation energy of 1.31 ± 0.06 eV for decay to $I^- + I_2(X\,^1\Sigma_g^+)$. From this value, the spin–orbit coupling constant of the iodine atom, the dissociation energies of I_2 and I_2^-,[26,27] and the term energies of the *A* and *B* states of I_2,[28,29] one can construct the energy level diagram for I_3^- and its possible photofragments, Fig. 1. The lower and upper bands of I_3^- are also depicted in Fig. 1. There are numerous decay pathways energetically accessible following excitation in the UV:

$$I_3^- \rightarrow I^-(^1S) + I_2(X\,^1\Sigma_g^+) \quad D_0 = 1.31 \pm 0.06 \text{ eV} \tag{1}$$

$$\rightarrow I(^2P_{3/2}) + I_2^-(X\,^2\Sigma_u^+) \quad D_0 = 1.85 \pm 0.06 \text{ eV} \tag{2}$$

$$\rightarrow I^-(^1S) + I_2(A\,^3\Pi_{1u}) \quad D_0 = 2.66 \pm 0.06 \text{ eV} \tag{3}$$

$$\rightarrow I^*(^2P_{1/2}) + I_2^-(X\,^2\Sigma_u^+) \quad D_0 = 2.79 \pm 0.06 \text{ eV} \tag{4}$$

$$\rightarrow I^-(^1S) + 2I(^2P_{3/2}) \quad D_0 = 2.85 \pm 0.06 \text{ eV} \tag{5}$$

$$\rightarrow I^-(^1S) + I_2(B\,^3\Pi_{0u}^+) \quad D_0 = 3.26 \pm 0.06 \text{ eV} \tag{6}$$

$$\rightarrow I^-(^1S) + I(^2P_{3/2}) + I^*(^2P_{1/2}) \quad D_0 = 3.80 \pm 0.06 \text{ eV} \tag{7}$$

Time- and frequency-domain experiments on the photodissociation and photoelectron spectroscopy of I_3^- have been carried out in our laboratories.[1,30,31] The time-resolved photodissociation of gas phase I_3^- at 390 nm was studied by Zanni *et al.*[30] using femtosecond photoelectron (FPE) spectroscopy. Excitation of I_3^- at this wavelength resulted in the production of I^- and I_2^- with approximately equal yields. The FPE spectra showed that the I_2^- photoproduct was vibrating coherently with $\langle v\rangle = 67$, a considerably higher value than observed in solution. Zanni *et al.* constructed a collinear

[a]Current address: School of Chemistry and Physics, University of Adelaide, SA, 5005, Australia.
[b]Author to whom correspondence should be addressed. Electronic mail: dan@radon.cchem.berkeley.edu

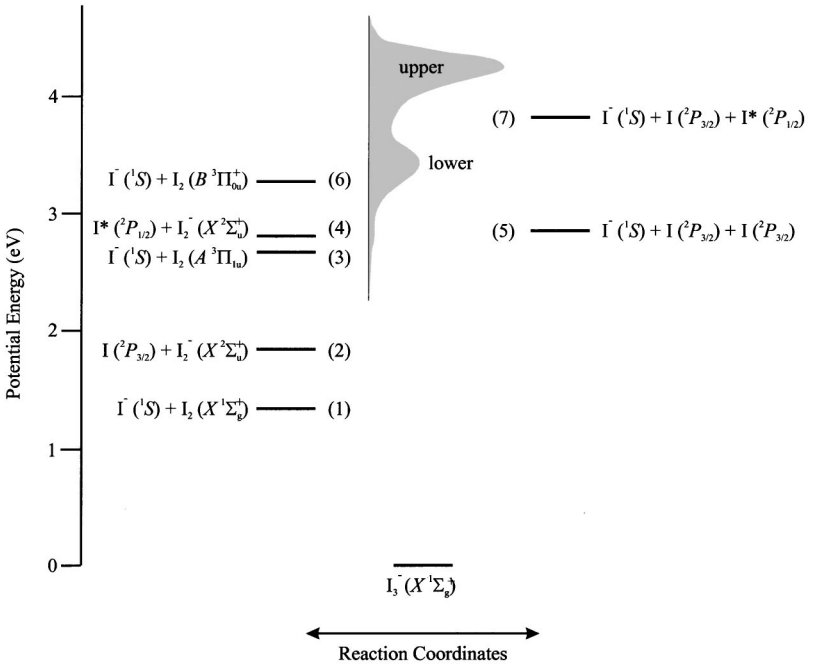

FIG. 1. Energy level diagram for I_3^- indicating the ground state of I_3^- relative to the asymptotic energies of the fragment channels. Two-body dissociation channels are presented to the left of I_3^- and three-body dissociation channels to the right. The shaded area represents the photofragment yield spectrum of gas-phase I_3^- as reported in Ref. 2.

excited state potential energy surface that reproduced the observed level of I_2^- excitation in quantum wave packet simulations. These simulations also indicated that the I^- was generated via three-body dissociation, rather than from an $I_2 + I^-$ product channel.

Choi *et al.*[1] carried out further investigations of the photodissociation spectroscopy and dynamics of gas phase I_3^- in the range of 240–420 nm. The photofragment yield (PFY) spectrum of I_3^- revealed two intense features with maxima at 290 and 360 nm, in accordance with solution phase work. Additionally, coincidence detection of the photofragments using two-particle time- and position-sensing (TPS) (Ref. 32) at several wavelengths yielded product branching ratios and translational energy $[P(E_T)]$ distributions. These results demonstrated that both two- and three-body dissociation occurred over the entire wavelength range, as evidenced by photoproduct mass ratios of 1:2 and 1:1. The two-body products from both the lower and upper bands were assigned to a combination of $I + I_2^-(X\,^2\Sigma_u^+)$ and $I^* + I_2^-(X\,^2\Sigma_u^+)$. However, only the mass ratio of these products (and not the charge state) was unambiguously identified in these experiments. Three-body dissociation was shown to occur through synchronous concerted dissociation of I_3^-, with the central iodine atom having little momentum in the center-of-mass frame. Finally, branching ratios between the two- and three-body channels indicated that the two-body dissociation fraction varied from 45% to 67%, depending on photon energy.

Zhu *et al.*[2] have carried out a complementary study of I_3^- photodissociation, in which the anion products from the dissociation of I_3^- were monitored by photofragment mass spectrometry, yielding the I^- and I_2^- branching fractions from 270 to 540 nm. Their PFY spectrum was quite similar to that obtained by Choi *et al.*,[1] but the $I_2^-:I^-$ ratio for the lower band was considerably smaller than the two-body:three-body ratio found by Choi. As a result, Zhu *et al.* proposed that the two-body channel seen by Choi *et al.* from the lower band was a combination of $I^- + I_2$ and $I + I_2^-$ products. This interpretation is supported indirectly by the recent theoretical work of Vala *et al.*[21] on the ground and excited state potentials of I_3^-. These calculations show that there are extensive curve-crossings among the numerous excited state potentials, implying that all energetically allowed dissociation channels should occur to some extent.

In this paper, we report results on the photodissociation of I_3^- obtained with a recently installed photofragment coincidence imaging detector.[33] The new design presents several advantages, described in more detail in the following section, over that used in the work of Choi *et al.*[1] In particular, the new detector is not restricted to the detection of only two fragments per laser shot, and charged fragments can be detected directly. These features result in better characterization of both the two- and three-body dissociation channels of I_3^-. The new results provide evidence for $I^- + I_2(A\,^3\Pi_{1u})$ production following excitation of the lower band, which accounts for some of the discrepancies in the branching ratios between the two earlier photodissociation studies.[1,2] In addition, we find no evidence for production of $I^* + I_2^-(X\,^2\Sigma_u^+)$ from excitation of the lower band, nor of $I + I_2^-(X\,^2\Sigma_u^+)$ from the upper band, in contrast to our earlier work. Finally, we obtain considerably more information on the decay dynamics of the three-body channels.

II. EXPERIMENT

The current photodissociation experiments were performed on our fast beam photofragment translational spectrometer. The ion beam, mass-spectrometer, and laser interaction components of this instrument[32,34,35] remain unchanged from our earlier study of I_3^-,[1] but the TPS detector[33] is quite different.

Rotationally and vibrationally cooled I_3^- is produced by flowing argon gas (14 psi) over iodine crystals at room tem-

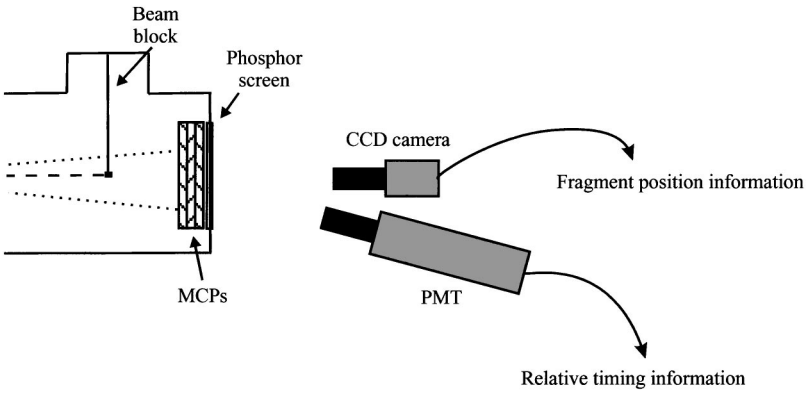

FIG. 2. Schematic diagram of the coincidence imaging detector. The paths of the photofragments and parent anion are represented by dotted and dashed lines, respectively.

perature and supersonically expanding the resulting gas mixture through a pulsed piezoelectric valve. A 1 keV electron beam intersects the free jet expansion downstream of the valve orifice. The resulting anions are accelerated to a known laboratory beam energy between 7 and 9 keV and mass-selected using a Bakker time-of-flight mass spectrometer, which imparts negligible kinetic energy spread to the ion beam.[36,37] An excimer-pumped dye laser with a bandwidth of 0.3 cm^{-1} is used to dissociate mass-selected ions at a specific photon energy. The photofragments then strike a microchannel plate (MCP) detector assembly with TPS capabilities for each fragment. A movable beam block in front of the detector prevents undissociated ions from impacting the MCPs. Consequently, any observed signal is due to the recoiling photoproducts.

The TPS detector in use, Fig. 2, is a coincidence imaging detector based on the design by Amitay and Zajfman.[38] In this detection scheme, the MCP assembly is coupled to a phosphor screen. Each photofragment that impacts the MCP assembly produces a spot on the phosphor screen that is then detected by a charge-coupled device (CCD) camera and a multianode photomultiplier tube (PMT). The positions of the fragments are obtained from the CCD camera, while the PMT provides relative timing information. For each dissociation event, the masses of the photoproducts, center-of-mass translational energy release E_T, and, for two-body dissociation, recoil angle θ are obtained from the fragments' positions and arrival times. For three-body dissociation, the center-of-mass momenta of all three particles are determined. Based on the $P(E_T)$ distribution resulting from the dissociation of $O_2\, B\, ^3\Sigma_u^-\, (v'=7)$, the current translational energy resolution of this arrangement is $\Delta E_T/E_T \approx 0.7\%$.[33]

The beam block reduces the detection efficiency of those fragments that have low translational energy or values of θ close to 90° with vertically polarized laser light, while fragments of high translational energy with θ close to 0° or 180° miss the detector entirely. These effects are accounted for by normalizing the raw translational energy distributions with a detector acceptance function (DAF) for decay yielding two fragments.[32] The $P(E_T)$ distributions from two-body dissociation reported here have been corrected with the DAF. Owing to the increased detector area and reduced size of the beam block as compared to the prior TPS detector, the DAF is relatively constant over the energy range for both two- and three-body dissociation of I_3^- for which two fragments are detected. The three-body distributions presented are the raw $P(E_T)$ distributions.

The new detector presents several advantages with respect to the I_3^- experiment. First, the front MCP of the previous TPS detector,[32] which employed a dual wedge-and-strip anode for time- and position-sensing, was biased at a high negative potential, precluding the detection of anions. Therefore, coincidence detection of all photofragments resulting from anion photodissociation required that any anionic fragments be photodetached by absorption of an additional photon. In the case of I_3^-, all of the photodissociation studies[1] were carried out at photon energies above the electron affinities of I and I_2 (3.0591 eV and 2.524 eV, respectively[39]), so that detachment of the anionic fragments was energetically feasible. Nonetheless, this requirement was an undesirable feature because one had to assume in constructing the $P(E_T)$ distributions that the detachment cross sections for the I_2^- photofragments were independent of internal excitation. In the new detector design, the front MCP is at ground potential, which allows anionic (and neutral) fragments to be detected directly.

In addition, the previous TPS detector was restricted to the detection of two photofragments per laser shot. Synchronous concerted three-body dissociation of I_3^- was inferred from events in which the photofragment mass ratio was 1:1. For such an event, the two detected fragments corresponding to the outer I atoms were approximately equally displaced from the center of the detector, while the third fragment, corresponding to the central I atom, impacted the beam block. The new detector permits the detection of three photofragments per dissociation event, as was demonstrated in our recent study of $I_2^- \cdot Ar$ photodissociation,[33] yielding a more complete picture of the three-body decay channel.

III. RESULTS

The photodissociation of I_3^- was investigated at photon energies ranging from 3.18 to 4.28 eV (390–290 nm). There are three possible types of valid events that can result from the dissociation of I_3^-: (i) two-body dissociation to $I^- + I_2$ or $I + I_2^-$, which will give rise to a photofragment mass ratio of 1:2, (ii) three-body dissociation with all three fragments detected, and (iii) three-body decay in which one of the fragments either strikes the beam block or is not detected due to less than unit detection efficiency, yielding a photofragment

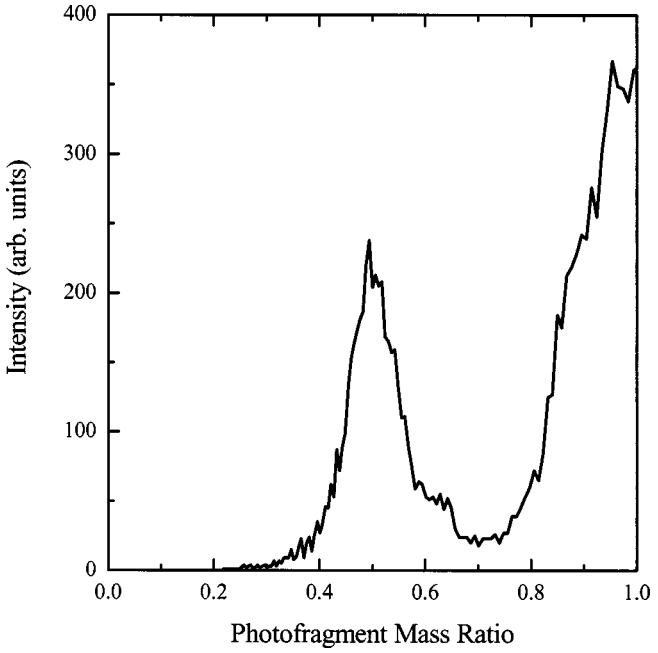

FIG. 3. Photofragment mass ratio of two-fragment valid events following excitation of I_3^- at 3.64 eV.

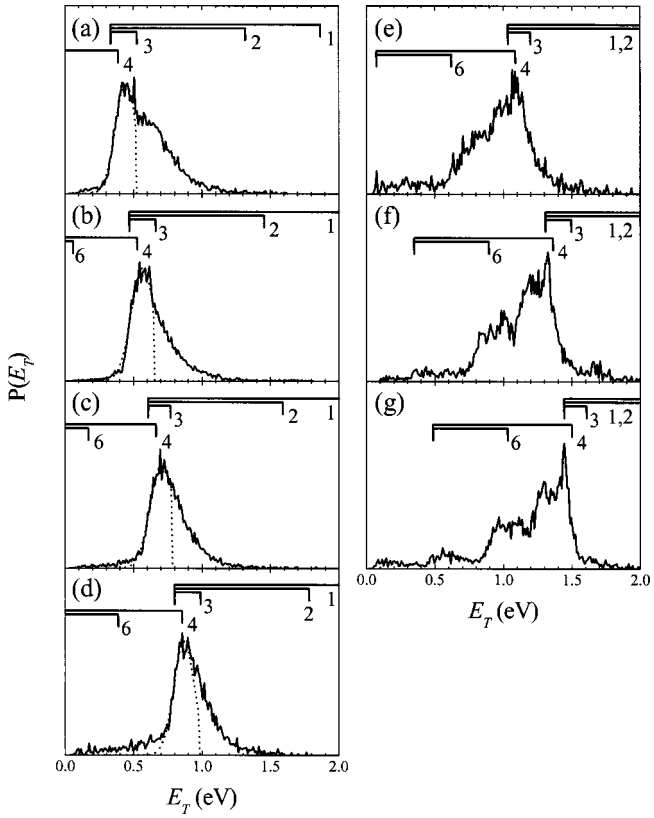

FIG. 4. Photofragment translational energy distributions for two-body dissociation of I_3^- (solid curves). The allowed translational energies for channels (1)–(4) and (6) are bracketed. The dotted lines represent the fit of the observed $P(E_T)$ distributions to Gaussian distributions for channel (3) that have been truncated at E_T^{max} for channel (3). Photon energies in eV are (a) 3.18, (b) 3.31, (c) 3.44, (d) 3.64, (e) 3.87, (f) 4.15, and (g) 4.28.

mass ratio of 1:1. From this point forward, the terms ''two-fragment'' and ''three-fragment'' will refer to the detection of two and three photoproducts from a dissociation event, while the ''two-body'' and ''three-body'' dissociation channels are those generating two and three iodine fragments regardless of the number detected. At each excitation energy, all three types of events are observed. Figure 3 presents an example (at $h\nu = 3.64$ eV) of photoproduct mass ratios for valid coincidence events resulting in the detection of two fragments, and demonstrates well-separated contributions from mass ratios 1:2 and 1:1.

The photofragment $P(E_T)$ distributions for the 1:2 mass ratio products are presented in Fig. 4; Figs. 4(a)–4(d) correspond to the lower band, Figs. 4(f)–4(g) to the upper band, and Fig. 4(e) to the minimum between the bands (see Fig. 1). The brackets in each panel represent the allowed translational energies between the maximum and minimum, E_T^{max} and E_T^{min}, for channels (1)–(4) and (6). The values for E_T^{max} are determined from the dissociation energies presented in Sec. I, while E_T^{min} corresponds to an internal energy that is equal to the bond dissociation energy of the diatomic fragment. Within each band, the distributions shift towards higher E_T with increasing photon energy. However, there is a qualitative change in the contours between the two bands. In the lower band, no signal is seen below E_T^{min} for channels (1)–(3), while in the upper band, no signal is seen above E_T^{max} for channel (4). Hence, excitation of the two bands leads to markedly different two-body channel distributions.

Figure 5 shows the $P(E_T)$ distributions for the three-body dissociation products when either two or three fragments are detected (dotted and solid lines, respectively) and reflects the relative number of two- and three-fragment events at each photon energy. The vertical arrows denote the expected kinetic energy release based on the dissociation energies for channels (5) and (7). Channel (7), which is accessible at the two highest photon energies, is evident as a very small amount of two-fragment signal. As with the two-body dissociation channel, the $P(E_T)$ distributions shift to higher translational energy with increasing photon energy. The three-fragment distributions are generally broader than the two-fragment distributions, but they become narrower with increasing excitation energy. Furthermore, the fraction of three-body dissociation events for which all three fragments are detected generally increases with photon energy, as shown in Table I.

The $P(E_T)$ distributions presented in Figs. 4 and 5 differ from those previously reported by Choi *et al.*[1] In that work, the $P(E_T)$ distributions for the photofragments with a mass

TABLE I. Branching fractions for detection of two and three fragments from the three-body dissociation of I_3^-.

Photon energy (eV)	2 fragments	3 fragments
3.18	0.74	0.26
3.31	0.81	0.19
3.44	0.58	0.42
3.64	0.52	0.48
3.87	0.48	0.52
4.15	0.36	0.64
4.28	0.39	0.61

ratio of 1:2 exhibited two features throughout the upper and lower bands, labeled A and B, that were assigned to the $I + I_2^-(X\,^2\Sigma_u^+)$ and $I^* + I_2^-(X\,^2\Sigma_u^+)$ channels, respectively. In the current study, the distributions in Figs. 4(a)–4(d) are quite similar to feature A, but feature B formerly seen at low E_T is absent. In the upper band, we now find feature A at high energy to be missing, and the minimum energy at which signal is observed is considerably higher than in our earlier study. In addition, the new distributions for the 1:1 mass ratio events are considerably cleaner; the earlier results showed a continuum rising toward low E_T that is not present in the current data.

Finally, analysis of the photofragment angular distributions yields an average anisotropy parameter[40] of $\beta = 1.4 \pm 0.2$ for both the 1:2 and 1:1 mass channels throughout the photon energy range probed. This value is consistent with previous results indicating that transitions to the upper and lower bands are parallel.[1,5]

IV. ANALYSIS

A. Two-body dissociation

The photofragment translational energy distributions originating from excitation of the lower band of I_3^-, Figs. 4(a)–4(d), are peaked in the region of $E_T^{\min}$ for the $I^- + I_2(X\,^1\Sigma_g^+)$, $I + I_2^-(X\,^2\Sigma_u^+)$, and $I^- + I_2(A\,^3\Pi_{1u})$ channels, indicating an internally excited diatomic fragment. The sharp decrease in intensity below $E_T^{\min}$ signifies that one or more of these channels contribute to the distributions, and that the $I^* + I_2^-(X\,^2\Sigma_u^+)$ and $I^- + I_2(B\,^3\Pi_{0u}^+)$ channels are absent. At a photon energy of 3.18 eV [Fig. 4(a)], the $P(E_T)$ distribution has two partially resolved features; one between $E_T^{\min}$ and $E_T^{\max}$ for channel (3), $I^- + I_2(A\,^3\Pi_{1u})$, and a second feature that extends to considerably higher energy, but not beyond $E_T^{\max}$, for channel (2), $I + I_2^-(X\,^2\Sigma_u^+)$. Hence, we assign the lower energy feature to channel (3) and the higher energy feature to vibrationally and rotationally excited $I_2^- + I$. These two contributions are apparent but less resolved at 3.31 eV [Fig. 4(b)]. In Figs. 4(c) and 4(d), the two channels can no longer be resolved and the distributions appear as a single feature that is likely a combination of channels (2) and (3). There is no evidence for channel (1), $I^- + I_2(X\,^1\Sigma_g^+)$, in the form of signal at $E_T > E_T^{\max}$ for channel (2), although there could be a contribution from this channel with very highly excited I_2.

The $P(E_T)$ distributions from the upper band, Figs. 4(f) and 4(g), exhibit broader features that extend to $E_T^{\max}$ for channel (4), $I^* + I_2^-(X\,^2\Sigma_u^+)$. The relatively sharp onset to dissociation in the region of maximum kinetic energy release for this channel and the near lack of signal in the region corresponding to channels (1)–(3) indicate that channel (4) has become the principal dissociation pathway. The photofragment translational energy distributions reveal greater intensity near $E_T^{\max}$ for channel (4), signifying less vibrational excitation in the diatomic fragment than for channel (2) from the lower band. There is intensity in the energetically allowed region for channel (6), $I^- + I_2(B\,^3\Pi_{0u}^+)$; thus, this channel may contribute as well. Finally, excitation at the photon energy that lies between the two bands results in a $P(E_T)$ distribution, Fig. 4(e), that appears to have contributions from channels (2), (3), and (4).

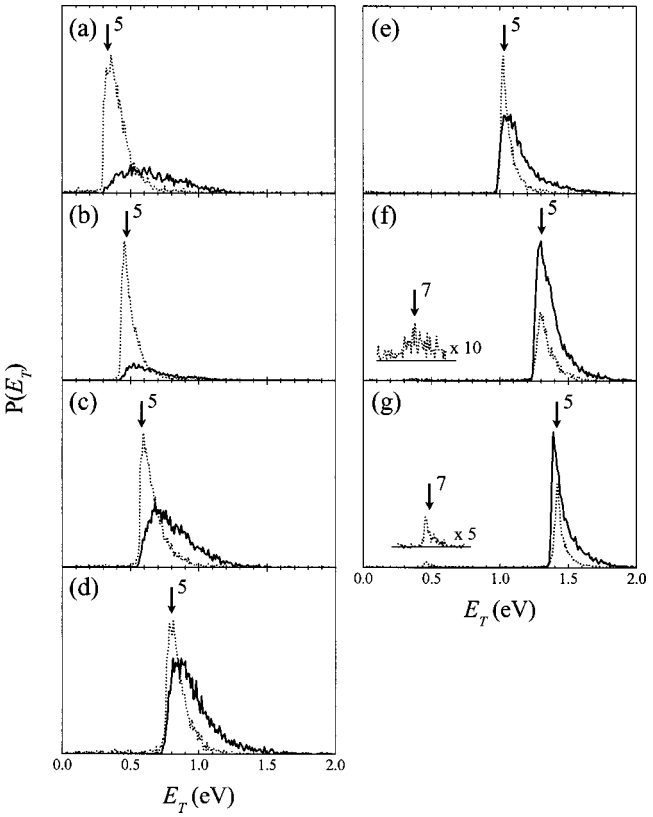

FIG. 5. Photofragment translational energy distributions for three-body dissociation of I_3^-. The expected kinetic energy release for channels (5) and (7) are indicated by vertical arrows. The solid and dotted lines represent the distributions resulting from the detection of all three and two fragments, respectively. Photon energies in eV are (a) 3.18, (b) 3.31, (c) 3.44, (d) 3.64, (e) 3.87, (f) 4.15, and (g) 4.28.

B. Three-body dissociation

At all excitation energies, channel (5), $I^- + 2I(^2P_{3/2})$, is the dominant three-body dissociation pathway. The $P(E_T)$ distributions resulting from this channel should appear at a single energy, but the results in Fig. 5 clearly show that the two- and three-fragment distributions extend asymmetrically towards values of E_T that are higher than expected. This observation is attributed to internal excitation of the I_3^- in the ion beam. However, one would also like to understand why the three-fragment signal becomes more dominant at higher photon energies (Table I), why the three-fragment distributions generally extend to higher E_T, and why the two- and three-fragment distributions differ the most at the lowest photon energies.

These trends can be explained as follows. Two-fragment events with photofragment mass ratios of 1:1 result from dissociation trajectories in which the center-of-mass momenta of the two outer I atoms are nearly equal and opposite; the central iodine has very little momentum and strikes the beam block. In a three-fragment event, the central I atom must have enough momentum to scatter out of the beam, miss the beam block, and impact the detector. For ions with

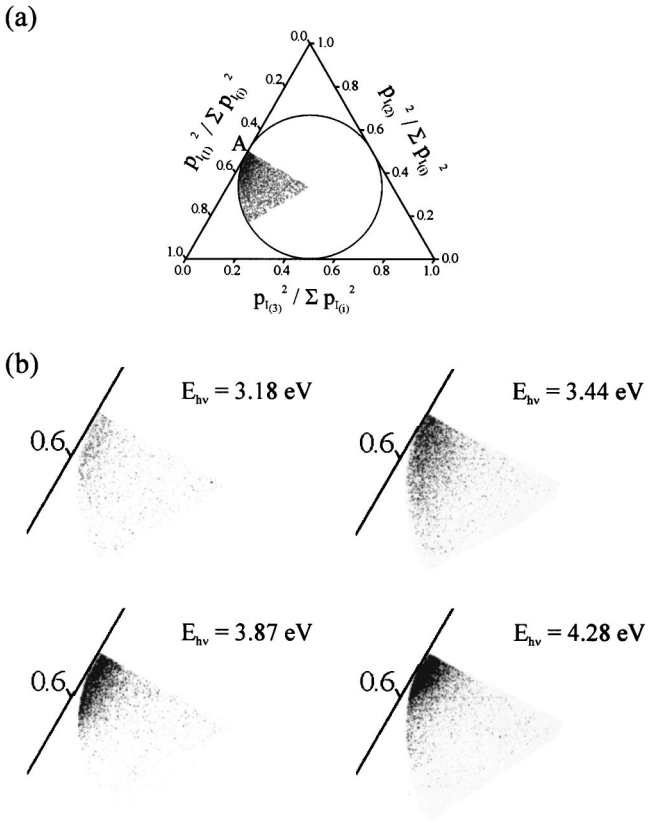

FIG. 6. Dalitz plots of momentum partitioning among the three fragments in the three-body dissociation of I_3^-. (a) Due to conservation of momentum and energy, all points must lie within the circle inscribed in the triangle. The notation $I_{(i)}$ in the axis labels indicates the relative momenta of the three fragments, with "1" being the highest and "3" being the lowest. Point A corresponds to those events with zero momentum for $I_{(3)}$ and equal but opposite momenta in the remaining two I fragments. The photon energy is 3.18 eV. (b) Enlarged view of the Dalitz plots at selected photon energies.

no initial internal energy, three-fragment events become more likely at higher photon energies, since more translational energy is available to all three photofragments. At a fixed photon energy, photodissociation of internally excited ions should also favor three-fragment over two-fragment events, especially if the bending and antisymmetric stretching modes of the ions are excited. Thus, at the lowest photon energies in Fig. 5, three-body photodissociation of cold ions leads preferentially to two-fragment events, while only those ions that are vibrationally hot yield three-fragment events. Consequently, the $P(E_T)$ distributions for two- and three-fragment events differ the most at low photon energy. As the photon energy is raised, three-fragment events become possible for a larger fraction of the total ensemble of ions, resulting in the observation of a higher fraction of three-fragment events and a reduction in the differences between the $P(E_T)$ distributions from two- and three-fragment events.

The three-fragment events can be analyzed with the aid of the Dalitz plots[41–43] presented in Fig. 6. These plots illustrate the momentum partitioning among the three fragments for each dissociation event. Conservation of momentum and energy dictate that all events lie within the inscribed circle in Fig. 6(a). Moreover, as the three fragments from the dissociation of I_3^- are indistinguishable in the current experiment, the momentum partitioning exhibits sixfold symmetry,[44–46] and all events can be plotted in one-sixth of the inscribed circle. Figure 6(b) shows the relevant sector of the Dalitz plots at higher magnification for four photon energies. Point A represents synchronous concerted dissociation from a linear geometry in which both I–I bonds break simultaneously. This produces two fragments with equal and opposite momenta and a third that has zero momentum. There is intensity not only in the region of point A, but also extending slightly away from point A, which corresponds to events in which one of the fragments has very low momentum and there is unequal momentum partitioning between the remaining two iodine atoms. The implications of the Dalitz plots will be discussed in Sec. V.

TABLE II. Branching fractions for two- and three-body dissociation of I_3^- and I_2^-:I^- branching ratio.

Photon energy (eV)	Two-body	Three-body	I_2^-:I^-
3.18	0.64	0.36	1:1.7
3.31	0.60	0.40	1:3.2
3.44	0.49	0.51	1:3.6
3.64	0.37	0.63	1:4.9
3.87	0.30	0.70	1:2.3
4.15	0.45	0.55	1:1.2
4.28	0.45	0.55	1:1.2

C. Branching fractions

The branching fractions for the two- and three-body dissociation channels were calculated at all photon energies investigated, with the results presented in Table II. The two-body dissociation channel is represented by all two-fragment events with a 1:2 mass ratio, while the three-body channel is the sum of the three-fragment events and the 1:1 mass ratio two-fragment events. At all but the lowest two photon energies, three-body dissociation is the favored decay pathway. Additionally, the results in Table II reveal a decrease in the fraction of two-body dissociation signal with increasing excitation energy within the lower band. The last column, listing the I_2^-:I^- branching ratios, is obtained using the procedure described in Sec. V.

D. Comparison to earlier results

The results reported in this section differ in several respects from those previously reported.[1] We formerly asserted that both $I+I_2^-(X\,^2\Sigma_u^+)$ and $I^*+I_2^-(X\,^2\Sigma_u^+)$ were produced regardless of which band was excited, in contrast to the assignments in Sec. IV A. The source of this discrepancy lies in the detection method employed in the previous study. As discussed in Sec. II, the TPS detector used in the earlier work precluded the direct detection and analysis of anion photoproducts; photodetachment of an electron from the anion fragment was required for detection. If a single dissociation event occurred without detachment, then the detection of a lone fragment would not constitute a coincidence event. However, in the instance that two dissociation events resulted from a single laser shot with detection of only the

neutral fragments, then these detected fragments would be treated as a coincidence event in the experiment. While many such occurrences were discarded as false coincidences, a significant number were accepted by the discrimination routine, particularly at low E_T where the displacements of the fragments from the center of the detector are small. Thus, we attribute the differences between the previously reported two-body $P(E_T)$ distributions[1] and those currently presented to these false coincidences in which in which two tri-iodide anions were dissociated but the anion fragments were not detected. Consequently, the previous conclusion that the $I+I_2^-(X\,^2\Sigma_u^+)$ and $I^*+I_2^-(X\,^2\Sigma_u^+)$ channels were present at all photon energies is incorrect. False coincidences of this type also gave rise to the intensity at low E_T in the 1:1 mass ratio $P(E_T)$ distributions of Choi *et al.*[1] that does not appear in the current results.

The improved analysis procedure afforded by the new detector results in different branching fractions for the two- and three-body decay channels than those previously reported.[1] While we originally claimed that two-body dissociation was more prevalent from 3.44 to 4.15 eV, we now find that three-body decay is the dominant channel in this energy range.

V. DISCUSSION

The current experiments demonstrate that two- and three-body dissociation occur in both the upper and lower bands of gas phase I_3^-. In the lower band, the observed $P(E_T)$ distributions for two-body dissociation comprise contributions from the $I+I_2^-(X\,^2\Sigma_u^+)$ and $I^-+I_2(A\,^3\Pi_{1u})$ channels, while in the upper band, the primary two-body dissociation channel is the $I^*+I_2^-(X\,^2\Sigma_u^+)$ channel with the possibility of a contribution from the $I^-+I_2(B\,^3\Pi_{0u}^+)$ channel. The three-body decay process, $I^-+2I(^2P_{3/2})$, is present at all excitation energies; it is the predominant channel throughout the upper band and at higher energies within the lower band. The $P(E_T)$ distributions within the lower band extend down to $E_T^{\min}$ for channels (2) and (3), indicating that the I_2 or I_2^- fragments are produced with internal energies from zero to their dissociation energies, after which point three-body dissociation occurs. Hence, there appears to be a smooth transition from two- to three-body dissociation within the lower band. The $P(E_T)$ distributions for the upper band, on the other hand, are most intense near $E_T^{\max}$ for channel (4), indicating significantly less internal excitation of the I_2^- product than for channel (2) from the lower band.

It is of interest to compare the branching fractions for the two- and three-body decay channels in Table II to the I^- and I_2^- branching fractions of Zanni *et al.*[30] and Zhu *et al.*[2] If one were to assume that three-body dissociation is the sole source of I^-, then the $I_2^-:I^-$ ratio would be identical to the two-body:three-body branching ratio. At 3.18 eV (390 nm), the two-body:three-body ratio reported in Table II is 1.8:1. Zanni *et al.* found approximately equal production of I_2^- and I^-, while Zhu *et al.* determined the $I_2^-:I^-$ ratio to be approximately 1:4. Zhu *et al.* also reported a decrease in the $I_2^-:I^-$ ratio across the lower band profile, reaching values as low as 1:10 around 3.7 eV. They pointed out that for the lower band, their I_2^- branching fractions were significantly lower than our previously reported two-body fractions,[1] and proposed that this discrepancy resulted from a contribution to the two-body signal from a channel yielding I^-. The improved two-body branching fractions in Table II of this paper are closer to the I_2^- branching fractions of Zhu *et al.* but remain higher for all photon energies of the lower band. With this in mind, we can examine the composition of the two-body channel more closely and try to reconcile the various measurements.

As discussed in Sec. IV A, there is strong evidence that channel (3), $I^-+I_2(A\,^3\Pi_{1u})$, contributes to the two-body signal, particularly at an excitation energy of 3.18 eV where there are two distinct contributions to the $P(E_T)$ distribution, Fig. 4(a). If 22% of the total two-body signal in Fig. 4(a) is from channel (3), with the remainder from channel (2), then the $I_2^-:I^-$ ratio would be unity, in agreement with the results of Zanni *et al.*, whereas 69% of this signal would have to originate from channel (3) to match the results of Zhu *et al.* at 3.18 eV. By fitting the $P(E_T)$ distribution in Fig. 4(a) with the assumptions that the contribution from channel (3) is a truncated Gaussian whose contour matches the $P(E_T)$ distribution at low E_T, and that the remainder of the photofragment translational energy distribution arises from channel (2), we find that 43% of the signal is due to channel (3). The resulting $I_2^-:I^-$ ratio, 1:1.7, lies between the values obtained by Zanni *et al.* and Zhu *et al.* A similar analysis of the data in Figs. 4(b)–4(d) yields channel (3) contributions of 60%, 56%, and 54%, respectively. The curves used to obtain these values are depicted as dotted lines in Figs. 4(a)–4(d) and have been truncated at $E_T^{\max}$ for channel (3). The resulting $I_2^-:I^-$ ratios, presented in Table II, are now close to (although systematically slightly higher than) the ratios obtained by Zhu *et al.* Therefore, the two sets of measurements are largely consistent provided that channel (3) is the two-body source of I^-. The remaining differences may result from either the uncertainty associated with this analysis, as the contributions from channels (2) and (3) are not cleanly resolved in Figs. 4(b)–4(d), or from a small contribution to the two-body signal from channel (1) with highly excited I_2.

In the upper band, our branching fractions for two- and three-body decay are in accordance with the I_2^- and I^- branching fractions measured by Zhu *et al.* This is consistent with our assignment of the two-body channel as $I^*+I_2^-(X\,^1\Sigma_g^+)$. A small contribution to the two-body signal from channel (6) would yield slightly better agreement, but the discrepancies are not large enough to confirm the presence of channel (6).

Looking more globally at the two-body channels, our finding that excitation of the lower band yields ground state iodine atoms while excitation of the upper band produces $I^*(^2P_{1/2})$ atoms is consistent with some of the earliest correlations proposed for I_3^- photodissociation,[47] as well as the recent adiabatic potentials calculated by Vala *et al.*[21] using the diatomics-in-molecules (DIM) approximation including spin–orbit coupling. However, as pointed out by those authors, there are significant problems with the DIM curves for I_3^-, including an inverted ordering of the excited $^3\Pi_u$ and

$^1\Sigma_u^+$ states responsible for the lower and upper bands, respectively.

Assignment of the $I^- + I_2(A\,^3\Pi_{1u})$ channel as a significant decay pathway from the lower band represents a new wrinkle on the overall dynamics. The potential energy curves in the Franck–Condon region for excitation of I_3^- calculated by Vala *et al.*[21] demonstrate that the lower optically active excited state lies very close to two potential energy curves that correlate to the $I^- + I_2(A\,^3\Pi_{1u})$ channel asymptote. Thus, nonadiabatic coupling to these states may be responsible for the production of channel (3). In contrast, the upper state dissociation dynamics appear to be more adiabatic from the perspective of two-body dissociation, with $I^* + I_2^-(X\,^1\Sigma_g^+)$ being the dominant products.

Turning to three-body dissociation, the current results, in which both two- and three-fragment events are detected, yield a more complete picture of the overall dynamics than was possible in our previous study[1] that only permitted the detection of two-fragment events. The previous work was strongly biased towards detection of synchronous concerted dissociation of I_3^- with equal momentum partitioning between the observed iodine fragments. One can now determine, by means of the Dalitz plots in Fig. 6, the extent to which this type of dissociation dominates the three-body channel.

The interpretation of Dalitz plots for the case of three particles of equal mass has been discussed at length by Muller *et al.*,[44] Babikov *et al.*,[45] and others.[42,46,48] Each point within the inscribed circle represents a mapping of the center-of-mass momentum vectors for the three photofragments, subject to the constraint that the sum of the vectors is zero. As mentioned in Sec. IV B, point A in Fig. 6(a) corresponds to two atoms having equal and opposite momentum and the third having zero momentum, the result expected for synchronous concerted dissociation of a linear triatomic molecule. As one moves from point A towards the center of the circle, the three-body dissociation becomes progressively less collinear; the tips of the three vectors evolve from a line to an obtuse isosceles triangle, becoming an equilateral triangle at the center. On the other hand, moving along the diameter of the circle away from point A corresponds to all three vectors being collinear but increasingly unequal in magnitude, representing progressively more asymmetric collinear dissociation.

Figure 6 shows that at 3.18 eV, events are scattered throughout the sector of the inscribed circle but are most dense in the region near point A, indicating the presence of synchronous concerted dissociation from linear I_3^-. Additionally, Fig. 6(b) illustrates that the concentration of events in this region of low momentum for the lowest momentum fragment increases with photon energy, corresponding to a greater proportion of three-fragment events originating from cold I_3^- as was discussed in Sec. IV B. The Dalitz plots also reveal a number of events corresponding to noncollinear and asymmetric collinear dissociation. Thus, the bending and antisymmetric stretching vibrations of I_3^- are influencing the decay dynamics through both zero point motion and initial population of excited vibrational levels.

Overall, the Dalitz plots not only demonstrate that the synchronous concerted decay mechanism previously inferred from the two-fragment measurements is largely valid, but also more accurately and completely reflect the dissociation dynamics. The plots result from a single decay mechanism with the internal motion of I_3^- causing the distribution to be spread about point A. There is no evidence of a competing mechanism, such as sequential or asynchronous concerted decay, as was observed in the collisional dissociation of Na_3^+.[45] A secondary decay mechanism of this type would yield an additional region of intensity on the diameter of the inscribed circle removed from point A. In addition, the relatively smooth evolution of the Dalitz plots from the lower band to the upper band suggests similar decay dynamics for channel (5) regardless of which electronic state is excited. Thus, it appears that the initial symmetric stretch motion on the two excited states, as evidenced by the symmetric stretch progressions in the resonance Raman spectra of I_3^-,[7–9] maps onto the asymptotic three-body dissociation dynamics.

VI. CONCLUSIONS

The photodissociation dynamics of gas phase I_3^- have been examined using a fast beam photofragment translational spectrometer coupled to a coincidence imaging detector that enables the direct detection and analysis of two and three neutral or anion fragments from single dissociation events. The new detection scheme results in a more complete and accurate picture of the dissociation dynamics than we obtained in an earlier study.[1]

Throughout the entire energy range investigated, 3.18–4.28 eV, two- and three-body dissociation channels are detected, with three-body dissociation dominating at all but the lowest photon energy. Although many decay pathways are energetically accessible at the excitation energies employed in this study, the two-body fragmentation from the lower band leads mainly to the production of $I(^2P_{3/2}) + I_2^-(X\,^2\Sigma_u^+)$ and $I^- + I_2(A\,^3\Pi_{1u})$, and the upper band results in $I^*(^2P_{1/2}) + I_2^-(X\,^2\Sigma_u^+)$ photofragments. The assignment of a significant fraction of the two-body products from the lower band to $I^- + I_2(A\,^3\Pi_{1u})$ yields branching fractions for I_2^- and I^- that are consistent with those measured by Zhu *et al.*[2] by photofragment tandem mass spectrometry.

Finally, the observed three-body decay at all photon energies arises primarily from $I^- + 2I(^2P_{3/2})$ photoproducts. Analysis of the three-body events using Dalitz plots illustrates that the three-body decay dynamics are dominated by synchronous concerted dissociation but are influenced by the reactant bend and antisymmetric stretch vibrational motions.

ACKNOWLEDGMENTS

This research was supported by the Director, Office of Basic Energy Science, Chemical Sciences Division of the U.S. Department of Energy under Contract No. DE-AC03-76SF00098. K.E.K. is a National Science Foundation Predoctoral Fellow.

[1] H. Choi, R. T. Bise, A. A. Hoops, and D. M. Neumark, J. Chem. Phys. **113**, 2255 (2000).
[2] L. Zhu, K. Takahashi, M. Saeki, T. Tsukuda, and T. Nagata, Chem. Phys. Lett. **350**, 233 (2001).
[3] A. D. Awtrey and R. E. Connick, J. Am. Chem. Soc. **73**, 1842 (1951).
[4] T. Okada and J. Hata, Mol. Phys. **43**, 1151 (1981).
[5] M. Mizuno, J. Tanaka, and I. Harada, J. Phys. Chem. **85**, 1789 (1981).
[6] H. Isci and W. R. Mason, Inorg. Chem. **24**, 271 (1985).
[7] K. Kaya, N. Mikami, M. Ito, and Y. Udagawa, Chem. Phys. Lett. **16**, 151 (1972).
[8] W. Kiefer and H. J. Bernstein, Chem. Phys. Lett. **16**, 5 (1972).
[9] A. E. Johnson and A. B. Myers, J. Phys. Chem. **100**, 7778 (1996).
[10] A. E. Johnson and A. B. Myers, J. Chem. Phys. **104**, 2497 (1996).
[11] U. Banin, A. Waldman, and S. Ruhman, J. Chem. Phys. **96**, 2416 (1992).
[12] U. Banin and S. Ruhman, J. Chem. Phys. **98**, 4391 (1993).
[13] U. Banin and S. Ruhman, J. Chem. Phys. **99**, 9318 (1993).
[14] E. Gershgoren, E. Gordon, and S. Ruhman, J. Chem. Phys. **106**, 4806 (1997).
[15] T. Kuhne and P. Vohringer, J. Chem. Phys. **105**, 10788 (1996).
[16] T. Kuhne and P. Vohringer, J. Phys. Chem. A **102**, 4177 (1998).
[17] T. Kuhne, R. Kuster, and P. Vohringer, Chem. Phys. **233**, 161 (1998).
[18] I. Benjamin, U. Banin, and S. Ruhman, J. Chem. Phys. **98**, 8337 (1993).
[19] G. Ashkenazi, R. Kosloff, S. Ruhman, and H. Talezer, J. Chem. Phys. **103**, 10005 (1995).
[20] R. M. Lynden-Bell, R. Kosloff, S. Ruhman, D. Danovich, and A. Vala, J. Chem. Phys. **109**, 9928 (1998).
[21] J. Vala, R. Kosloff, and J. N. Harvey, J. Chem. Phys. **114**, 7413 (2001).
[22] D. Danovich, J. Hrusak, and S. Shaik, Chem. Phys. Lett. **233**, 249 (1995).
[23] S. B. Sharp and G. I. Gellene, J. Phys. Chem. **101**, 2192 (1997).
[24] C. J. Margulis, D. F. Coker, and R. M. Lynden-Bell, J. Chem. Phys. **114**, 367 (2001).
[25] K. Do, T. P. Klein, C. A. Pommerening, and L. S. Sunderlin, J. Am. Soc. Mass Spectrom. **8**, 688 (1997).
[26] K. P. Huber and G. Herzberg, *Molecular Spectra and Molecular Structure IV Constants of Diatomic Molecules* (Van Nostrand Reinhold, New York, 1979).
[27] M. T. Zanni, T. R. Taylor, B. J. Greenblatt, B. Soep, and D. M. Neumark, J. Chem. Phys. **107**, 7613 (1997).
[28] D. R. T. Appadoo, R. J. LeRoy, P. F. Bernath, S. Gerstenkorn, P. Luc, J. Verges, J. Sinzelle, J. Chevillard, and Y. DAignaux, J. Chem. Phys. **104**, 903 (1996).
[29] P. Luc, J. Mol. Spectrosc. **80**, 41 (1980).
[30] M. T. Zanni, B. J. Greenblatt, A. V. Davis, and D. M. Neumark, J. Chem. Phys. **111**, 2991 (1999).
[31] T. R. Taylor, K. R. Asmis, M. T. Zanni, and D. M. Neumark, J. Chem. Phys. **110**, 7607 (1999).
[32] R. E. Continetti, D. R. Cyr, D. L. Osborn, D. J. Leahy, and D. M. Neumark, J. Chem. Phys. **99**, 2616 (1993).
[33] A. A. Hoops, J. R. Gascooke, A. E. Faulhaber, K. E. Kautzman, and D. M. Neumark, Chem. Phys. Lett. **374**, 235 (2003).
[34] D. J. Leahy, D. L. Osborn, D. R. Cyr, and D. M. Neumark, J. Chem. Phys. **103**, 2495 (1995).
[35] D. L. Osborn, H. Choi, D. H. Mordaunt, R. T. Bise, D. M. Neumark, and C. M. Rohlfing, J. Chem. Phys. **106**, 3049 (1997).
[36] J. M. B. Bakker, J. Phys. E **6**, 785 (1973).
[37] J. M. B. Bakker, J. Phys. E **7**, 364 (1974).
[38] Z. Amitay and D. Zajfman, Rev. Sci. Instrum. **68**, 1387 (1997).
[39] J. C. Rienstra-Kiracofe, G. S. Tschumper, H. F. Schaefer, S. Nandi, and G. B. Ellison, Chem. Rev. **102**, 231 (2002).
[40] R. N. Zare, Mol. Photochem. **4**, 1 (1972).
[41] R. H. Dalitz, Philos. Mag. **44**, 1068 (1953).
[42] L. M. Wiese, O. Yenen, B. Thaden, and D. H. Jaecks, Phys. Rev. Lett. **79**, 4982 (1997).
[43] C. Maul and K. H. Gericke, J. Phys. Chem. **104**, 2531 (2000).
[44] U. Muller, T. Eckert, M. Braun, and H. Helm, Phys. Rev. Lett. **83**, 2718 (1999).
[45] D. Babikov, E. A. Gislason, M. Sizun, F. Aguillon, V. Sidis, M. Barat, J. C. Brenot, J. A. Fayeton, and Y. J. Picard, J. Chem. Phys. **116**, 4871 (2002).
[46] T. G. Clements, A. K. Luong, and R. E. Continetti, Chem. Phys. Lett. **366**, 650 (2002).
[47] D. Meyerstein and A. Treinin, Trans. Faraday Soc. **59**, 1114 (1962).
[48] D. Strasser, L. Lammich, S. Krohn, M. Lange, H. Kreckel, J. Levin, D. Schwalm, Z. Vager, R. Wester, A. Wolf, and D. Zajfman, Phys. Rev. Lett. **86**, 779 (2001).